Title:

Electrokinetic, electrochemical and electronic surface potentials of the pristine water liquid-vapor interface

Author(s):

Maximilian R. Becker, Philip Loche, Roland R. Netz

Electrokinetic, electrochemical and electronic surface potentials of the pristine water liquid-vapor interface

Maximilian R. Becker, Philip Loche, Roland R. Netz

April 13, 2022

Abstract

Although conceptually simple, the air-water interface displays rich behavior. Different definitions of the electrostatic potential, each relevant for distinct experimental scenarios, lead to widely varying surface potential magnitudes and even different signs. Based on quantum-chemical density-functional molecular dynamics simulations, all relevant surface potentials are evaluated and compared. The spatially averaged surface potential, accessible to electron holography, is dominated by the trace of the water molecular quadrupole moment and amounts to more than + 4 V inside the water phase, very different from results obtained with force-field water models. The surface potential inside a cavity is much smaller, less than 200 mV in magnitude, and depends specifically on the cavity radius. This is the electrochemical surface potential relevant for ion transfer reactions and ion surface adsorption. Charge transfer between water molecules leads to pronounced surface potentials as well. However, when probing electrophoresis by explicitly applying a lateral electric field, the zeta potential turns out to be zero. Thus, charge transfer between water molecules does not translate to a non-zero electrophoretic mobility at the pristine vapor-liquid water interface.

1 Introduction

At charged surfaces that are in contact with an aqueous salt solution, an ionic double layer forms, which determines the electrostatic potential difference between the surface and the solution surface, called the surface potential. Even at the nominally uncharged air-water interface, different ions exhibit different interfacial affinities, which gives for most ion combinations rise to a pronounced ionic charge distribution normal to the interface and thus to a non-vanishing surface potential. Since even pure water contains ions due to the autoprotolysis, this mechanism is operative also in the absence of added salt.

But a surface potential is also present in the absence of ions at all, due to the molecular water dipole in conjunction with an anisotropic water orientation at the interface and due to the quadrupolar charge distribution within a water molecule. It follows that both the dipole and the quadrupole moment of water contributes to the surface potential.[1,2] The laterally averaged surface potential of liquid water from density-functional-theory molecular-dynamics (DFT-MD) simulations was determined to be +3.1 V and +3.6 V,[3,4] in good quantitative agreement with electron holography measurements of vitrified ice.[5,6] Employing a similar experimental technique, the surface potential of liquid water has recently been experimentally determined to be +4.48 V.[7] In contrast, simple three-point-charge force-field molecular-dynamics (FF-MD) simulations yield a negative surface potential in the range of -0.4 V to -0.6 V, yet the interfacial water structure is rather similar for DFT-MD and FF-MD simulations of the air-water interface.[8] This behavior can be shown to be due to the trace of the water quadrupolar tensor, which is very different for different water models and dominates the surface potential but does not influence the water-water interactions and thus is irrelevant for the interfacial water structure.[2,9,10]

There are different ways of experimentally measuring the electrostatic surface potential, which all give rise to significantly different values, hence, different experimental measurements in fact define different surface potentials.

In electrochemical experiments, electrostatic potential differences acting on finite size ions are reported. They fundamentally differ from the above-mentioned electron holography experiments, since ions do not probe the interior electrostatic potentials of water molecules, the electrochemical

potential therefore does not reflect the spatially averaged electrostatic potential across an interface. Moreover, water molecules are anisotropically oriented around ions, which gives rise to an additional electrostatic potential contribution. Thus, in the hypothetical experiment where an ion crosses the air-water interface, the electrostatic work done on the ion charge results from the sum of the air-water surface potential and the potential across the ion hydration shell.[11–13] It follows that the quadrupolar water contribution to the electrochemical potential cancels out, which explains why force-field and DFT simulations give quite comparable results for electrochemical potential across the air-water interface.[9,13,14]

Surface potentials have also been determined from the kinetic energy loss of high-energy electrons[15] or helium nuclei[16] that cross the air-water interface. Depending on their kinetic energy, the particles do also probe the electrostatics inside the water molecules. However, it should be noted that the ionizing radiation has to cross two interfaces, namely the air-water interface and the water-substrate interface to the radioactive source or to the detector, depending on the experimental setup. In any case, what is measured in these experiments is not the absolute surface potential of the air-water interface but rather the surface potential difference between the air-water interface and a water-solid interface.

In x-ray photoelectron spectroscopy[17] and second harmonic generation[18] the situation is again different: here, the electrostatic potential is probed at positions inside the water molecules that reflect the average position of the electrons that are involved.

Experimentally very easy to measure is the electrophoretic or electro-osmotic mobility of a particle or a surface. By using a number of approximations and assumptions, this mobility can be converted into the electrostatic potential difference between the bulk liquid phase and the shear plane at which the liquids fulfills a no-slip boundary condition, which defines the so-called ζ – potential. It is long known that the pristine vapor-water interface exhibits a negative ζ – potential,[19–22] which in early works was interpreted in terms of an enhanced interfacial adsorption of hydroxide ions with respect to hydronium ions. This interpretation however contradicts the experimentally fact that the surface tension of acids decreases and of bases increases with concentration, which indicates that hydronium has a slight propensity to bind to the vapor-solution interface, while hydroxide is slightly repelled from the vapor-solution interface,[8,23] as confirmed by sum frequency generation and second harmonic generation experiments[24] as well as simulations.[8,25] Alternative explanations for the negative ζ – potential of neat water invoke the adsorption of negatively charged surface-active impurities, which are omnipresent even in pure lab water,[26,27] although it should be noted that this interpretation is controversially discussed.[28] It also has been suggested that the water dipolar orientation at the water-vapor surface, which gives rise to a dipolar potential distribution, leads to an electrophoretic mobility, but in later simulation and analytic work it was shown that a pure orientation of water molecules cannot lead to stationary electroosmotic flow.[29] According to yet another interpretation, the ζ – potential of the pristine air-water interface is produced by intermolecular charge transfer due to an asymmetry of the spatial distribution of hydrogen-bond donating and accepting water molecules close to the vapor-water interface, which causes an inhomogeneous charge distribution.[30–32] This prompts the question whether intermolecular charge transfer can principally give rise to electrophoretic motion.

2 Results

To study the different potentials of the neat vapor-water interface we conduct DFT-MD simulations of the system shown in Fig. 1a, containing 352 water molecules in a simulation box of 2 nm x 2 nm x 6 nm that form a stable vapor-liquid water slab geometry as shown by the density profile in Fig. 1b. The DFT-MD density profile (red line) displays oscillations on a short spatial scale that reflects water layering and is due to the short sampling time, as demonstrated by comparison with FF-MD simulations of the same system size but over much longer times (black line, see SI for an in-depth discussion). If charge transfer produced mobile charges that can move in response to an external electric field, a tangential electric field would perform work on these charges and produce a net shear flow at the interface, corresponding to a finite ζ - potential. In order to study the electrophoretic mobility, we apply an electric field of $E_{\parallel} = 257$ mV/nm parallel to the interface and record the induced water motion. The same simulation procedure has been used to calculate ζ – potentials at lipid bilayers using FF-MD.[33] The treat-

ment of finite electric fields as implemented in the software package CP2K accounts for the Berry phase[34] and has been successfully applied to the auto-dissociation of liquid water[35] and to Raman spectroscopy.[36] We obtain the mean water velocity profile $u(z)$, based on the molecular center-of-mass velocities, depicted in Fig. 1d (red circles, left scale), which is zero within the numerical error. We now establish the theoretical basis to convert the water flow profile to experimentally reported ζ – potentials.

For a mobile charge density profile $\rho_{\mathrm{mob}}(z)$ in the water phase and in the presence of a tangential electric field $E_{\parallel}$, the hydrodynamic flow at the interface is governed by the Stokes equation[37]

$$\frac{d}{dz}\left[\eta_{\perp}(z)\frac{d}{dz}u(z)\right] = -E_{\parallel}\rho_{\mathrm{mob}}(z)\,, \qquad (1)$$

where $\eta_{\perp}(z)$ is the water viscosity profile and $u(z)$ is the velocity profile. Using the definition of the perpendicular displacement field $dD_{\perp}(z)/dz = \rho_{\mathrm{mob}}(z)$, the local approximate relation between displacement and electric field $\varepsilon_0\varepsilon_{\perp}(z)E_{\perp}(z) = D_{\perp}(z)$, which defines the dielectric profile $\varepsilon_{\perp}(z)$, and the definition of the electrostatic potential $d\phi(z)/dz = -E_{\perp}(z)$, Eq. 1 is integrated twice to obtain

$$\phi(z) = \int_{z_1}^{z} \frac{\eta_{\perp}(z')}{E_{\parallel}\varepsilon_0\varepsilon_{\perp}(z')}\frac{du(z')}{dz'}\mathrm{d}z'\,, \qquad (2)$$

with the bulk value $\phi(z_1) = 0$ and where we assumed that the viscous stress vanishes in the interior of the liquid, $du(z)/dz|_{z=z_1} = 0$.

In the analysis of experimental electrophoretic data, the permittivity and viscosity profiles of water are assumed constant and set equal to their bulk values $\varepsilon_{\perp}(z) = \varepsilon_{\mathrm{bulk}}$ and $\eta_{\perp}(z) = \eta_{\mathrm{bulk}}$, which leads to the standard expression

$$\phi(z) = \frac{\eta_{\mathrm{bulk}}}{\varepsilon_0\varepsilon_{\mathrm{bulk}}E_{\parallel}}\left[u(z) - u(z_1))\right]\,. \qquad (3)$$

Using the experimental values for the bulk dielectric constant $\varepsilon_{\mathrm{bulk}} = 80$[38] and shear viscosity $\eta_{\mathrm{bulk}} = 0.85$ mPa·s[39] of water, we obtain the right potential scale in Fig. 1d. The shear viscosity of BLYP water was recently analyzed in the high frequency regime and found to be similar to the Tip4p/2005 force-field model, which is known to reproduce experimental values quite well.[40] We define the bulk water velocity $u(z_1)$ as the mean water velocity in the range $z - z_{\mathrm{GDS}} < -0.63$ nm. On solid surfaces, the ζ – potential is defined as the potential at the shear surface, where the velocities of the solid and the water phase are identical. At the vapor-liquid interface the ζ – potential corresponds to the velocity of the vapor phase relative to the bulk liquid, which corresponds to a subtle extrapolation since the water density goes to zero in the vapor phase. If we consider the two data points around the Gibbs dividing surface (GDS) in Fig. 1d, where the water density is between the liquid and vapor values, the ζ – potential is estimated to be at most of the order of -10 mV.

In order to scrutinize the connection between a possible electrophoretic water mobility and charge transfer, we calculate DDEC6 atomic charges every 100 frames of our DFT-simulations.[43] By adding up atomic charges for each water molecule we obtain the molecular charge density profile $\rho_{\mathrm{q,Mol}}(z)$ in Fig. 1f (blue spheres). Indeed, charge transfer gives rise to a local enrichment of positively charged water molecules at the vapor-water interface, accompanied by a broad negatively charged region in the the water phase, in agreement with previous approximate treatments.[30,32] Using Eq. 1, $\rho_{\mathrm{q,Mol}}(z)$ is converted into the velocity profile shown as a blue broken line in Fig. 1d. Indeed, charge transfer is predicted to produce a very tiny negative water flow on the liquid side of the GDS, which was previously associated with the experimentally measured negative ζ – potential of the vapor-water interface.[30] However, close to the GDS, the predicted water flow becomes positive and corresponds to a ζ – potential of +5 mV, much smaller than the experimental reports and in fact of opposite sign (note that the actual electrostatic potential created by the charged transfer profile $\rho_{\mathrm{q,Mol}}(z)$ is in fact larger by a factor of $\varepsilon_{\mathrm{bulk}} = 80$). We conclude that charge transfer does not produce electrophoresis on any relevant scale. Our calculated DDEC6 molecular charge profile is calculated from an equilibrium trajectory in the absence of an externally applied electrical field. In the SI we show that the DDEC6 charge profiles does not significantly change if an electric field of 257 mV/nm is applied.

The molecular charge density profile $\rho_{\mathrm{q,Mol}}(z)$ in Fig. 1f deviates from previous approximate results,[32] where the nuclear coordinates were sampled from FF-MD simulations. This is not surprising, since the interfacial structure of water deviates between DFT-MD and FF-MD simulations, which can be rationalized by polarization effects which are present in DFT-MD but missed in FF-MD simulations, see Fig. 1c. The interfacial water structure can be characterized by the

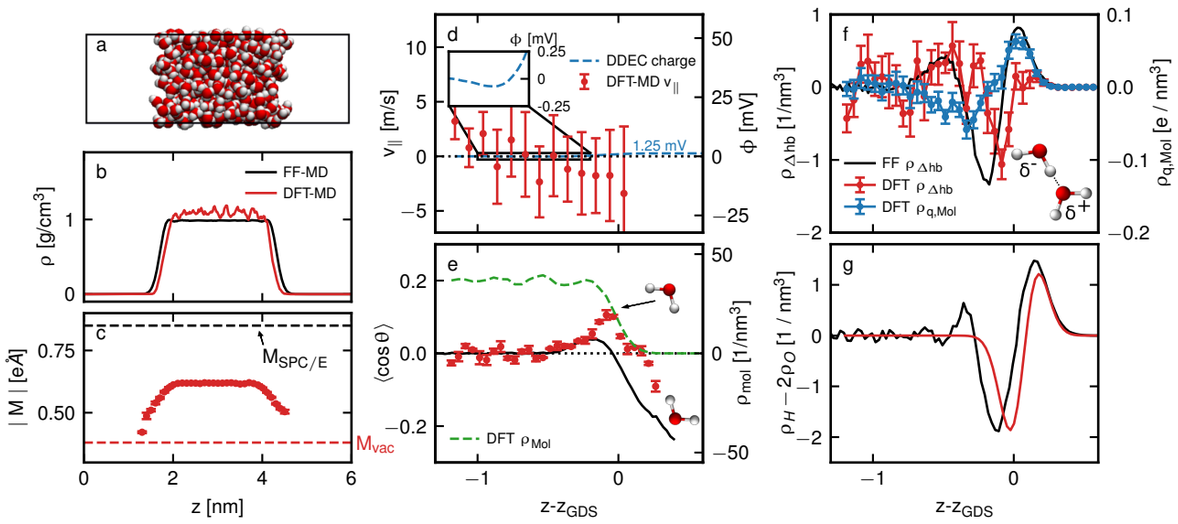

Figure 1: a. DFT-MD simulation snapshot of 352 water molecules that form a liquid slab in a box of 2 nm x 2 nm x 6 nm. b. Mass density profile from 100 ps DFT-MD (red) and 20 ns FF-MD (black) simulations, both with 352 water molecules. c. Water molecular dipole moment profile from DFT-MD (red circles). The bulk value of $M = 0.62$ eÅ and the vacuum value $M = 0.38$ eÅ (horizontal broken line) compare well to experimental values of 0.60±0.125 eÅ for liquid water[41] and 0.386 eÅ for vacuum.[42] The black broken line shows the dipole moment of the SPC/E FF model. d. Water velocity profile from DFT-MD for an applied tangential field of $E_\parallel = 257$ mV / nm (red points, left scale), the right scale shows the electrophoretic potential according to Eq. 3. The flow profile due to charge transfer between water molecules is shown by the blue broken line. e. Water orientational profile, where θ is the angle between the interface normal and the water dipoles, from DFT-MD (red circles) and FF-MD (black line). The green lines is the center-of-mass water density profile $\rho_{mol}(z)$ (right scale). f. Hydrogen bond balance $\rho_{\Delta\mathrm{hb}}(z)$ between accepted and donated hydrogen bonds, binned with respect to the water molecular center of mass from DFT-MD (red circles) and FF-MD (black line). The blue circles shows the molecular transfer charge density $\rho_{\mathrm{q,Mol}}(z)$ from a DDEC6 atomic charge analysis of the DFT-MD data. g. Hydrogen/oxygen density difference $\rho_{\mathrm{H}}(z) - 2\rho_{\mathrm{O}}(z)$ from DFT-MD (red line) and FF-MD (black line), binned with respect to individual atom positions.

orientational profile in terms of the mean of the cosine of the dipolar water angle with respect to the interface normal, $\langle\cos\theta\rangle$, shown in Fig. 1e. Both DFT-MD and FF-MD show that interfacial water points the H atoms to the vapor (negative $\langle\cos\theta\rangle$), followed by a layer towards the bulk water phase where the H atoms point to the liquid phase (positive $\langle\cos\theta\rangle$). We see that DFT water is more structured than SPC/E FF water and that the structuring extends further into the vapor phase. This shift into the vapor phase is also seen in the hydrogen-oxygen density difference profile shown in Fig. 1g. The overstructuring of our DFT simulations might be due to the BLYP exchange correlation functional we use.[44] Still, in both DFT and FF simulations, the hydrogen atoms of the top water layer are pointing towards the vapor phase, which produces OH-bonds that dangle into the vapor phase.[45]

To further understand the structural differences between FF-MD and DFT-MD simulations, we analyze the interfacial hydrogen bonding network. Charge transfer is interpreted in literature[30,31] to be caused by a broken symmetry between the number of accepted and donated hydrogen bonds per water molecule. We calculate the balance of accepted and donated hydrogen bonds according to

$$\rho_{\Delta\mathrm{hb}}(z) = \rho_{\mathrm{acc}}(z) - \rho_{\mathrm{don}}(z) \qquad (4)$$

by binning all water molecules with respect to their center of mass and adding +1 per accepted hydrogen bond and -1 per donated hydrogen bond. The results are shown in Fig. 1f. We employ the standard geometrical definition according to which a hydrogen bond exists if oxygen atoms are less than 3.5 Å apart and the O–H–O angle is higher than 150°.[46] The FF-MD hydrogen bond balance (black line in Fig. 1f) compares well to published data in the literature[30] and shows three pronounced extrema, similar to the hydrogen/oxygen density difference $\rho_{\mathrm{H}}(z) - 2\rho_{\mathrm{O}}(z)$

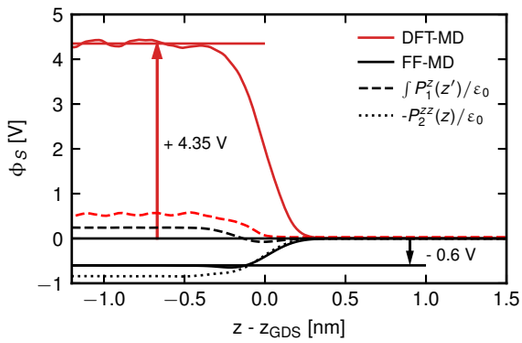

Figure 2: Comparison of the electrostatic surface potential calculated from FF-MD and DFT-MD simulations. For FF-MD simulations the contributions of the dipole density and quadrupole density are shown as dashed and dotted lines. For DFT-MD simulations only the dipolar contribution is shown.

in Fig. 1g. For the DFT data the agreement between the hydrogen bond balance (Fig. 1f red circles) and the hydrogen/oxygen density difference (Fig. 1g red curve) is less perfect than for the FF-MD data, but still, we conclude that the hydrogen-bond balance can to a large degree be explained by the profile of the hydrogen-oxygen density difference and thus by the interfacial water orientation. Note that in order to reduce the noise, we show in Fig. 1g a fit of the hydrogen/oxygen density difference from our DFT simulations (as explained in the SI). In agreement with our results, earlier ab-initio studies have predicted a small fraction of acceptor-only water molecules at the interface,[47] which is consistent with the hydrogen bond balance in Fig. 1f showing a rather weak maximum in the gas phase. We conclude that DFT and FF simulation show similar trends for the hydrogen-bond balance profile at the air-water interface, but for a quantitative charge-transfer analysis the full DFT analysis is needed. This follows from that rather pronounced deviation between the blue and red curves in Fig. 1f, which indicates that molecular charge transfer is not proportional to the hydrogen-bond balance.

We next analyze the laterally averaged electrostatic potential which results from the average interfacial polarization and includes nuclear and electronic effects. It is calculated by integrating the total charge density, in case of FF-MD only taking the point charges into account, in case of DFT-MD taking the distribution of electronic and core charges into account, see Methods. The data presented in Fig. 2 show that there is a large discrepancy between FF-MD and DFT-MD simulation results, as is well known. In agreement with literature, we find for the potential difference between vapor and liquid a value of +4.35 V for DFT-MD simulations and -0.6 V for FF-MD simulations with the SPC/E water model.[3,5] It has been established that the difference is mostly due to the difference in the trace of the water quadrupolar moment, which is irrelevant for the electrostatic interaction between water molecules. We therefore present in Fig. 2 also the dipolar density of the FF-MD and DFT-MD simulations, which are both positive and of roughly similar magnitude in the liquid phase. This reflects well the mean dipolar orientation of water molecules at the interface shown in Fig. 1e, which is rather similar for DFT and FF simulations. The quadrupolar contribution on the other hand is dominated by the molecular quadrupole moments, which differ strongly between the FF and DFT models. It is important to point out that our DFT method employs GTH pseudopotentials to represent the closed-shell electrons. This methods treats the resulting core charge within the Ewald construction as a smeared-out charge density. This treatment includes an approximation for the quadrupolar contribution of the atomic core. We compare the quadrupole moment of our DFT model with all electron calculations and find good agreement, see SI for more information.

Even though the interfacial potentials of FF and DFT water models are very different, these models still show similar interfacial structures and intermolecular interactions. The difference in the interface potentials has been rationalized by the fact that the lateral average of the electrostatic potential includes the atomic cores, which are highly charged in the DFT model.[5] It was shown that when averaging the DFT electrostatic potential only in the space between water molecules, a surface potential much closer to FF calculations is obtained. Here, we give a complementary picture. In Fig. 3b we show the electrostatic potential distribution inside a water molecule in the bulk liquid phase as a function of the position x_3 along the main bisector axis, as illustrated in the inset of Fig. 3c, from DFT-MD (red line) and FF-MD simulations (black line). Most notably, the potential diverges at the oxygen core position positively in DFT-MD and negatively in FF-MD, reflecting that the oxygen core charge is +6 e in DFT and -0.848 e for the SPC/E FF model.

At a distance to the oxygen core of $x_3 = -1.7$Å and $x_3 = 1.3$Å for FF-MD and $x_3 = -1.1$Å and $x_3 = 2.2$Å for DFT-

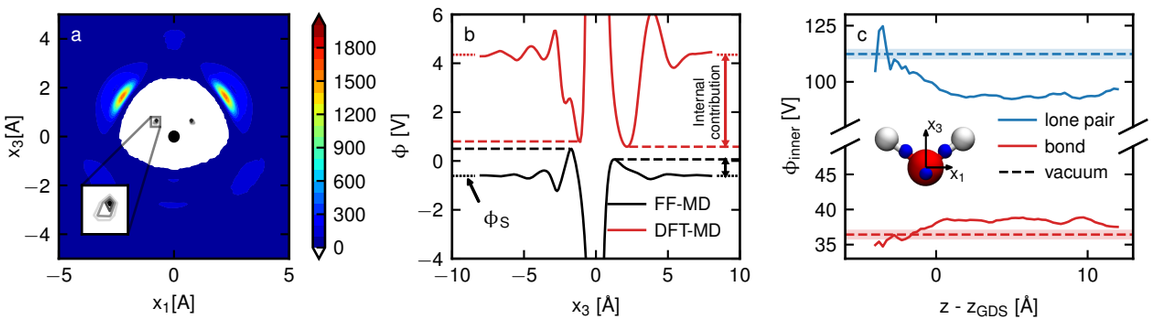

Figure 3: Electrostatic potential inside a water molecule. a. Number density of oxygen atom cores calculated from DFT-MD bulk water simulations as a function of the internal coordinate system of a water molecule in a water slab of 0.2 Å thickness in the H-O-H plane. b. Electrostatic potential averaged along the main bisector of a water molecule from FF-MD and DFT-MD simulations. c. Electrostatic potential evaluated at the Wannier centers of the bonding and lone-pair electrons as a function of the distance to the air-water interface.

MD we find the potential magnitudes to be minimal. These positions roughly correspond to the boundary between the central water molecules and the neighboring water molecules, as follows from the 2D resolved oxygen distribution function in Fig. 3a. At these positions the potentials are all positive and rather similar between DFT and FF, namely 0.78 V (DFT) and 0.5 V (FF) for negative x_3 and 0.58 V (DFT) to 0.06 V (FF) for positive x_3. This reflects that outside of the water molecule the different quadrupole moment of the DFT and FF models is largely irrelevant, the positive potential values reflect the positive interfacial dipolar contribution (note that the calculation is done for water molecules in the middle of a water slab). For larger distances from the oxygen core, the potential average over the interior of neighboring water molecules picks up quadrupolar contributions, which are positive for DFT-MD and negative for FF-MD, and asymptotically approaches the values of +4.35 for DFT-MD and -0.6 V for FF-MD, identical to the results in Fig. 2. In Fig. 3c we show the electrostatic potential at the position of Wannier centers of the bonding electrons (red line) and the lone-pair electrons (blue line) as a function of the position relative to the GDS of the vapor-water interface. As one moves into bulk, the electrostatic potential shifts away from the vacuum values and reaches a potential difference in bulk of $\phi_{\text{bulk}} - \phi_{\text{vac}} = 1.94$ V for bonding electrons and $\phi_{\text{bulk}} - \phi_{\text{vac}} = -18.2$ V for lone-pair electrons. These surface potentials are relevant for experimental techniques that couple to the water electrons in a surface-resolved manner, such as photo-electron spectroscopy or SFG. The results in Fig. 3 demonstrate how important the position relative to the water molecules is where the electrostatic potential is evaluated.

None of the electrostatic potentials analyzed so far reflects the electrostatic contribution to the work done when an ion approaches the air-water interface. This is so because when a finite-size ion is inserted into water, an oriented hydration layer forms around it which produces an electrostatic potential contribution inside the ion.[12,13,48–50] In order to extract the electrostatic potential, which corresponds to the linear electrostatic work contribution, it is sufficient to work with neutral cavities. As illustrated in Fig. 4a, we introduce single noble-gas atoms Helium, Neon, Argon and Krypton into the water-slab system at different separations from the interface and calculate the electrostatic potential excluding contributions from the noble-gas atom core and electrons (see Methods). In Fig. 4b we show the electrostatic potential from FF-MD on a line that passes through the center of an argon atom, as the air-water interface is crossed the potential drops to $\phi_S = -0.6$ V, but the interface around the atom largely compensates this potential and gives rise to a remaining electrochemical potential in the argon center of only $\phi_{EC} = -0.2$ V. In Fig. 4e and f we show the potential profile around different atoms in water bulk as a function of the radial distance from the atom center, where we put the potential in the atom center to be zero. For DFT-MD simulations we radially average the Hartree electrostatic potential output on a grid, for FF-MD simulations we solve the Poisson equation using the radially averaged water partial-charge distribution. The FF-MD profiles saturate for $r > 1.2$ nm, yielding the cavity-water potential ϕ_{CW} . The DFT-MD do not saturate at half of the used box length $L = 1.98$ nm, in

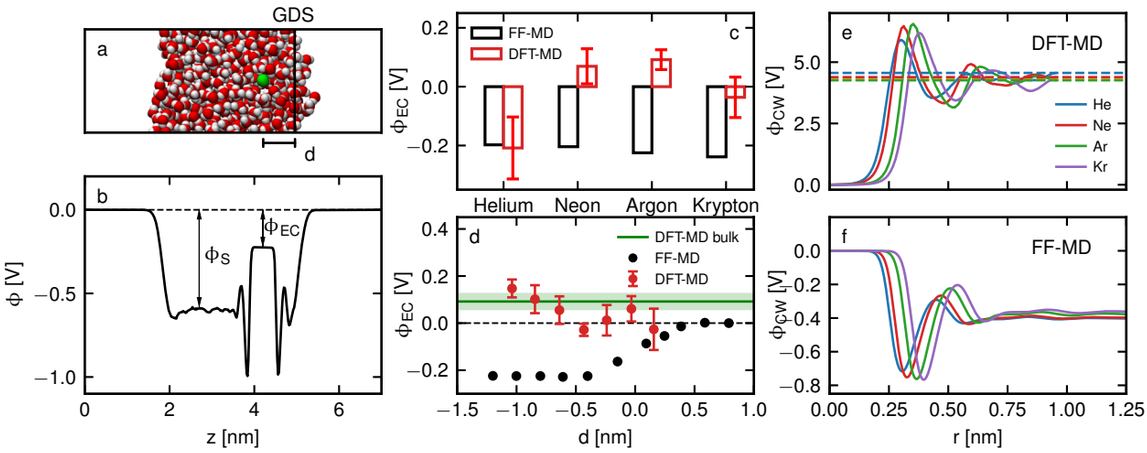

Figure 4: a. Snapshot from a FF-MD simulation of a single Argon atom in an air-water slab. b. Electrostatic potential profile of the system shown in (a) on a line through the Argon center, the surface potential ϕ_{S} and the electrochemical potential ϕ_{EC} are indicated. c. Electrochemical potential of different noble gas atoms. d. Electrochemical potential of an Argon atom as a function of the distance from the air-water interface. e. Electrochemical potential profiles from DFT-MD simulations. f. Electrochemical potential profiles from FF-MD simulations.

order to determine ϕ_{CW} we average the electrostatic potential for $r > L/2$, which results into the dashed lines in Fig. 4e. The electrochemical potential ϕ_{EC} follows from subtracting the cavity potential from the air-water surface potential

$$\phi_{\mathrm{EC}} = \phi_{\mathrm{S}} - \phi_{\mathrm{CW}} \tag{5}$$

and is shown in Fig. 4c for the different atoms used. First of all, the values of ϕ_{EC} are rather similar for FF and DFT simulations, showing that the huge differences in the air-water surface potentials indeed largely cancel out. The electrochemical potentials show a clear size dependence, which differs between FF-MD and DFT-MD simulations. For FF-MD simulations the neutral cavity potential decreases with increasing atom size, consistent with trends found for the neutral cavity potential of small ions,[51] the DFT-MD results however show a sign change when going from the smallest atom He to the larger atoms.

We also calculate the electrochemical potential profile by placing an Argon atom at different positions inside the air-water slab system. The potential profile from both DFT and FF simulations shows a smooth crossover from zero (in the vapor phase) to the value ϕ_{EC} in the bulk phase. The width of this crossover is roughly two times the width of the neat surface potential profile. From our DFT-MD data, we find a width of 0.29 nm for the surface potential profile in Fig. 2 and 0.63 nm for the neutral cavity potential profile

3 Conclusion

To address the different electrostatic potentials at the air-water interface from a unified perspective, we calculate potentials from DFT-MD as well as FF-MD simulations. In particular, we derive the ζ – potential from ab-initio simulations of an air-water interface by explicitly applying a tangential electric field. By this we show that although significant charge transfer takes place, the ζ – potential of the neat vapor-water interface is zero within the error bounds, suggesting that intermolecular charge transfer does not induce electrophoretic mobility. The laterally averaged surface potential from our DFT-MD simulations is +4.1 V, close to earlier theoretical work[3,4] and in good agreement with experimental electron holography measurements.[7] We also determine the surface potential within cavities of different size and for different separations from the air-water interface, which reflects the electrochemical potential acting on different ions. Finally, we evaluate the electrostatic potential acting on the lone-pair and the binding electrons within water molecules as a function of the separation from the interface. The picture that emerges from our simulations is that indeed different experiments probe vastly different surface potentials, which however can be all derived from suitably arranged simulations.

4 Acknowledgements

We acknowledge support by Deutsche Forschungsgemeinschaft, Grant CRC 1349, code 387284271, Project C04.

5 Methods

All FF-MD simulations have been conducted in Gromacs 2020 using the SPC/E water model with PME electrostatics and a 0.9 nm van-der-Waals cut-off. We employed a time step of 2 fs. DFT-MD simulations have been carried out using the CP2K 6.1 version[52] using the Born-Oppenheim approximation. We employed the BLYP functional with Grimme D3 dispersion correction,[53] GTH pseudopotentials and combine it with the DZVP-SR-MOLOPT basis set using a plane wave cutoff of 400Ry . All DFT-MD simulations use a time step of 0.5 fs.

DFT simulations employing the BLYP exchange correlation functional underestimate the density of liquid water quite substantially. Adding the Grimme dispersion correction usually changes this to an overestimated density.[44,54–56] In general, the density of ab-initio water depends quite strongly not only on the exchange correlation functional but also on the employed dispersion correction as well as the basis set. The DZVP-SR-MOLOPT basis set we employ in this work overestimates the density compared to previous studies using a TZV2P basis set which predicts values very close to the experimental ones, but nevertheless conserves structure and dynamics well.[44,57] In particular for the calculations of ζ – potentials long trajectories are needed, so we opted for the smaller basis set due to the gain in computational performance.

Vapor-Water slab simulations We conducted simulations of 352 water molecules in a periodic box of 2 nm x 2 nm x 6 nm resulting in a stable slab of roughly 3 nm thickness. We conducted a FF simulation with 1 ns equilibration time and subsequent production run of 20 ns. Using a FF-MD equilibrated configuration as input, we conducted 110 ps of DFT simulation of which we disregarded the first 10 ps for further equilibration purposes. We calculate molecular dipoles shown in Fig. 1c from the charge centers of maximally localized Wannier functions. The vacuum dipole moment has been calculated from a single water molecule in a $(1\ \mathrm{nm})^3$ cubic box in the NVT ensemble.

From the density profiles depicted in Fig. 1b we calculated the position of the GDS according to

$$z_{\mathrm{GDS}} = \int_{z_\mathrm{l}}^{z_\mathrm{v}} \frac{\rho_\mathrm{v} - \rho(z)}{\rho_\mathrm{v} - \rho_\mathrm{l}} \mathrm{d}z\,. \tag{6}$$

The electrostatic potential is evaluated from volumetric data that CP2K writes out. Directly averaging the potential gives identical results compared to writing out the full charge density and integrating according to Poisson equation. We fit the electrostatic potential profiles shown in Fig. 3 with tanh profiles. These fits result in the vapor-bulk potential differences 4.35V and -0.6V. All molecular properties, such as the molecular dipole moments in Fig. 1c, the velocity profile in Fig. 1d, orientational profiles in Fig.1e hydrogen bond balances in Fig. 1f and the quadrupolar and dipolar contributions shown in Fig. 2 are binned with respect to molecular center of masses.

Starting from a fully DFT-equilibrated system configuration we conducted a 120 ps simulation with an external E-field of $0.5 \cdot 10^{-4} \frac{\mathrm{E_h}}{\mathrm{ea_0}} \approx 257\mathrm{mV}$. Finite and periodic electric fields were applied according to the method introduced by Umari and Pasquarello.[34] We disregarded the first 25 ps of the simulation for equilibration purposes. This corresponds to a full relaxation of the in-field component of the total system polarization (see SI).

We calculate vacuum properties of water molecules such as the vacuum dipole moment and the interior potentials of water molecules under vacuum conditions from NVT single molecules DFT-MD simulations in a 2 nm x 2nm x 2nm sized box, sampling over 10 ps statistics.

Neutral cavity potentials We placed single argon atoms at different distances from the interface into a vapor water slab by replacing one of the water molecules of the slab shown in Fig. 1a. We conducted DFT simulations of these systems for at least 30 ps for each configuration and disregarded the first 5 ps in the evaluation. We evaluated the potential difference between the inner of the cavity and the vapor phase every 50 fs. For FF results we used a water slab of 648 water molecules. Since individual water molecules of the gas phase crossing over the periodic boundary conditions leads to a minor movement of the center of mass of the slab, we placed a solid wall at z=0 nm to repel water molecules. We collected 200 ns of statistics

for every distance and evaluated the neutral cavity potential with a Ewald - Summation of all charges in post processing.

References

[1] M. A. Wilson and A. Pohorille, "Comment on "Study on the liquid– vapor interface of water. I. Simulation results of thermodynamic properties and orientational structure"," *Journal of C*, p. 5211, 1989.

[2] D. J. Bonthuis, S. Gekle, and R. R. Netz, "Profile of the static permittivity tensor of water at interfaces: Consequences for capacitance, hydration interaction and ion adsorption," *Langmuir*, vol. 28, no. 20, pp. 7679–7694, 2012.

[3] K. Leung, "Surface potential at the air-water interface computed using density functional theory," *Journal of Physical Chemistry Letters*, vol. 1, no. 2, pp. 496–499, 2010.

[4] S. M. Kathmann, I. F. W. Kuo, and C. J. Mundy, "Electronic effects on the surface potential at the vapor-liquid interface of water," *Journal of the American Chemical Society*, vol. 130, no. 49, pp. 16556–16561, 2008.

[5] S. M. Kathmann, I. F. W. Kuo, C. J. Mundy, and G. K. Schenter, "Understanding the surface potential of water," *Journal of Physical Chemistry B*, vol. 115, no. 15, pp. 4369–4377, 2011.

[6] A. Harscher and H. Lichte *Proc. ICEM14*, vol. 1, p. 553, 1998.

[7] M. N. Yesibolati, S. Laganà, H. Sun, M. Beleggia, S. M. Kathmann, T. Kasama, and K. Mølhave, "Mean Inner Potential of Liquid Water," *Physical Review Letters*, vol. 124, no. 6, pp. 18–22, 2020.

[8] S. I. Mamatkulov, C. Allolio, R. R. Netz, and D. J. Bonthuis, "Orientation-Induced Adsorption of Hydrated Protons at the Air–Water Interface," *Angewandte Chemie - International Edition*, vol. 56, no. 50, pp. 15846–15851, 2017.

[9] R. C. Remsing, M. D. Baer, G. K. Schenter, C. J. Mundy, and J. D. Weeks, "The Role of Broken Symmetry in Solvation of a Spherical Cavity in Classical and Quantum Water Models," 2014.

[10] R. C. Remsing and J. D. Weeks, "The Influence of Distant Boundaries on the Solvation of Charged Particles," *Journal of Statistical Physics*, vol. 175, no. 3, pp. 743–763, 2019.

[11] P. Loche, C. Ayaz, A. Schlaich, D. J. Bonthuis, and R. R. Netz, "Breakdown of Linear Dielectric Theory for the Interaction between Hydrated Ions and Graphene," *Journal of Physical Chemistry Letters*, vol. 9, no. 22, pp. 6463–6468, 2018.

[12] T. T. Duignan, M. D. Baer, G. K. Schenter, and C. J. Mundy, "Real single ion solvation free energies with quantum mechanical simulation," *Chemical Science*, vol. 8, no. 9, pp. 6131–6140, 2017.

[13] T. L. Beck, "The influence of water interfacial potentials on ion hydration in bulk water and near interfaces," *Chemical Physics Letters*, vol. 561-562, pp. 1–13, 2013.

[14] T. T. Duignan, M. D. Baer, G. K. Schenter, and C. J. Mundy, "Electrostatic solvation free energies of charged hard spheres using molecular dynamics with density functional theory interactions," *Journal of Chemical Physics*, vol. 147, no. 16, 2017.

[15] N. L. Jarvis and M. A. Scheiman, "Surface potentials of aqueous electrolyte solutions," *Journal of Physical Chemistry*, vol. 72, no. 1, pp. 74–78, 1968.

[16] T. Adel, J. Velez-Alvarez, A. C. Co, and H. C. Allen, "Circuit Analysis of Ionizing Surface Potential Measurements of Electrolyte Solutions," *Journal of The Electrochemical Society*, vol. 168, no. 1, p. 016507, 2021.

[17] M. A. Brown, Z. Abbas, A. Kleibert, R. G. Green, A. Goel, S. May, and T. M. Squires, "Determination of surface potential and electrical double-layer structure at the aqueous electrolyte-nanoparticle interface," *Physical Review X*, vol. 6, no. 1, pp. 1–12, 2016.

[18] E. Ma and F. M. Geiger, "Divalent Ion Specific Outcomes on Stern Layer Structure and Total Surface Potential at the Silica:Water Interface," *Journal of Physical Chemistry A*, vol. 125, no. 46, pp. 10079–10088, 2021.

[19] S. Usui and H. Sasaki, "Zeta potential measurements of bubbles in aqueous surfactant solutions," *Journal of Colloid And Interface Science*, vol. 65, no. 1, pp. 36–45, 1978.

[20] S. Usui, H. Sasaki, and H. Matsukawa, "The dependence of zeta potential on bubble size as determined by the dorn effect," *Journal of Colloid And Interface Science*, vol. 81, no. 1, pp. 80–84, 1981.

[21] M. Takahashi, "ζ Potential of microbubbles in aqueous solutions: Electrical properties of the gas - Water interface," *Journal of Physical Chemistry B*, vol. 109, no. 46, pp. 21858–21864, 2005.

[22] C. Oliveira and J. Rubio, "Zeta potential of single and polymer-coated microbubbles using an adapted microelectrophoresis technique," *International Journal of Mineral Processing*, vol. 98, no. 1-2, pp. 118–123, 2011.

[23] L. M. Pegram and M. T. Record, "Partitioning of atmospherically relevant ions between bulk water and the water/vapor interface," *Proceedings of the National Academy of Sciences of the United States of America*, vol. 103, no. 39, pp. 14278–14281, 2006.

[24] R. J. Saykally, "Evidence for an enhanced proton concentration at the liquid water surface from SHG spectroscopy," *Optics InfoBase Conference Papers*, vol. 1460, pp. 7976–7980, 2007.

[25] V. Buch, A. Milet, R. Vácha, P. Jungwirth, and J. P. Devlin, "Water surface is acidic," *Proceedings of the National Academy of Sciences of the United States of America*, vol. 104, no. 18, pp. 7342–7347, 2007.

[26] Y. Uematsu, D. J. Bonthuis, and R. R. Netz, "Nanomolar Surface-Active Charged Impurities Account for the Zeta Potential of Hydrophobic Surfaces," *Langmuir*, vol. 36, no. 13, pp. 3645–3658, 2020.

[27] X. Yan, M. Delgado, J. Aubry, O. Gribelin, A. Stocco, F. Boisson-Da Cruz, J. Bernard, and F. Ganachaud, "Central Role of Bicarbonate Anions in Charging Water/Hydrophobic Interfaces," *Journal of Physical Chemistry Letters*, vol. 9, no. 1, pp. 96–103, 2018.

[28] S. Pullanchery, S. Kulik, H. I. Okur, H. B. De Aguiar, and S. Roke, "On the stability and necessary electrophoretic mobility of bare oil nanodroplets in water," *Journal of Chemical Physics*, vol. 152, no. 24, 2020.

[29] D. J. Bonthuis, D. Horinek, L. Bocquet, and R. R. Netz, "Electrohydraulic power conversion in planar nanochannels," *Phys. Rev. Lett.*, vol. 103, p. 144503, 2009.

[30] R. Vácha, O. Marsalek, A. P. Willard, D. J. Bonthuis, R. R. Netz, and P. Jungwirth, "Charge transfer between water molecules as the possible origin of the observed charging at the surface of pure water," *Journal of Physical Chemistry Letters*, vol. 3, no. 1, pp. 107–111, 2012.

[31] C. D. Wick, A. J. Lee, and S. W. Rick, "How intermolecular charge transfer influences the air-water interface," *Journal of Chemical Physics*, vol. 137, no. 15, 2012.

[32] E. Poli, K. H. Jong, and A. Hassanali, "Charge transfer as a ubiquitous mechanism in determining the negative charge at hydrophobic interfaces," *Nature Communications*, vol. 11, no. 1, pp. 1–13, 2020.

[33] A. Wolde-Kidan and R. R. Netz, "Interplay of Interfacial Viscosity, Specific-Ion, and Impurity Adsorption Determines Zeta Potentials of Phospholipid Membranes," *Langmuir*, vol. 37, no. 28, pp. 8463–8473, 2021.

[34] P. Umari and A. Pasquarello, "Ab initio Molecular Dynamics in a Finite Homogeneous Electric Field," *Physical Review Letters*, vol. 89, no. 15, pp. 1–4, 2002.

[35] A. M. Saitta, F. Saija, and P. V. Giaquinta, "Ab initio molecular dynamics study of dissociation of water under an electric field," *Physical Review Letters*, vol. 108, no. 20, pp. 1–5, 2012.

[36] A. Calzolari and M. B. Nardelli, "Dielectric properties and Raman spectra of ZnO from a first principles finite-differences/finite-fields approach," *Scientific Reports*, vol. 3, pp. 1–6, 2013.

[37] D. J. Bonthuis, S. Gekle, and R. R. Netz, "Dielectric profile of interfacial water and its effect on double-layer capacitance," *Physical Review Letters*, vol. 107, no. 16, pp. 1–5, 2011.

[38] C. Malmberg and A. Maryott, "Dielectric constant of water from 0 to 100 C," *Journal of Research of the National Bureau of Standards*, vol. 56, no. 1, p. 1, 1956.

[39] K. E. Bett and J. B. Cappi, "Effect of Pressure on the Viscosity of Water," *Nature*, vol. 207, pp. 620–621, 1965.

[40] A. P. Markesteijn, R. Hartkamp, S. Luding, and J. Westerweel, "A comparison of the value of viscosity for several water models using Poiseuille flow in a nano-channel," *Journal of Chemical Physics*, vol. 136, no. 13, pp. 1–17, 2012.

[41] Y. S. Badyal, M. L. Saboungi, D. L. Price, S. D. Shastri, D. R. Haeffner, and A. K. Soper, "Electron distribution in water," *Journal of Chemical Physics*, vol. 112, no. 21, pp. 9206–9208, 2000.

[42] S. A. Clough, Y. Beers, G. P. Klein, and L. S. Rothman, "Dipole moment of water from Stark measurements of H22O, HDO, and D2O," *The Journal of Chemical Physics*, vol. 2254, no. September, pp. 2254–2259, 1973.

[43] T. A. Manz and N. G. Limas, "Introducing DDEC6 atomic population analysis: Part 1. Charge partitioning theory and methodology," *RSC Advances*, vol. 6, no. 53, pp. 47771–47801, 2016.

[44] M. J. Gillan, D. Alfè, and A. Michaelides, "Perspective: How good is DFT for water?," *Journal of Chemical Physics*, vol. 144, no. 13, 2016.

[45] S. Sun, F. Tang, S. Imoto, D. R. Moberg, T. Ohto, F. Paesani, M. Bonn, E. H. Backus, and Y. Nagata, "Orientational Distribution of Free O-H Groups of Interfacial Water is Exponential," *Physical Review Letters*, vol. 121, no. 24, p. 246101, 2018.

[46] A. Luzar and D. Chandler, "Hydrogen-bond kinetics in liquid water," *Nature*, vol. 379, pp. 55–57, 1996.

[47] T. D. Kühne, T. A. Pascal, E. Kaxiras, and Y. Jung, "New insights into the structure of the vapor/water interface from large-scale first-principles simulations," *Journal of Physical Chemistry Letters*, vol. 2, no. 2, pp. 105–113, 2011.

[48] M. D. Baer, A. C. Stern, Y. Levin, D. J. Tobias, and C. J. Mundy, "Electrochemical surface potential due to classical point charge models drives anion adsorption to the air-water interface," *Journal of Physical Chemistry Letters*, vol. 3, no. 11, pp. 1565–1570, 2012.

[49] L. Horváth, T. Beu, M. Manghi, and J. Palmeri, "The vapor-liquid interface potential of (multi)polar fluids and its influence on ion solvation," *Journal of Chemical Physics*, vol. 138, no. 15, 2013.

[50] T. S. Hofer and P. H. Hünenberger, "Absolute proton hydration free energy, surface potential of water, and redox potential of the hydrogen electrode from first principles: QM/MM MD free-energy simulations of sodium and potassium hydration," 2018.

[51] S. J. Cox, D. G. Thorpe, P. R. Shaffer, and P. L. Geissler, "Assessing long-range contributions to the charge asymmetry of ion adsorption at the air-water interface," *Chemical Science*, vol. 11, no. 43, pp. 11791–11800, 2020.

[52] J. Hutter, M. Iannuzzi, F. Schiffmann, and J. Vandevondele, "Cp2k: Atomistic simulations of condensed matter systems," *Wiley Interdisciplinary Reviews: Computational Molecular Science*, vol. 4, no. 1, pp. 15–25, 2014.

[53] S. Grimme, J. Antony, S. Ehrlich, and H. Krieg, "A consistent and accurate ab initio parametrization of density functional dispersion correction (DFT-D) for the 94 elements H-Pu," *Journal of Chemical Physics*, vol. 132, no. 15, 2010.

[54] Z. Ma, Y. Zhang, and M. E. Tuckerman, "Ab initio molecular dynamics study of water at constant pressure using converged basis sets and empirical dispersion corrections.," *The Journal of chemical physics*, vol. 137, no. 4, p. 044506, 2012.

[55] M. Del Ben, M. Schönherr, J. Hutter, and J. Vandevondele, "Bulk liquid water at ambient temperature and pressure from mp2 theory," *Journal of Physical Chemistry Letters*, vol. 4, no. 21, pp. 3753–3759, 2013.

[56] M. Del Ben, J. Hutter, and J. VandeVondele, "Probing the structural and dynamical properties of liquid water with models including non-local electron correlation," *Journal of Chemical Physics*, vol. 143, no. 5, 2015.

[57] J. Schmidt, J. Vandevondele, I. F. William Kuo, D. Sebastiani, J. Ilja Siepmann, J. Hutter, and C. J. Mundy, "Isobaric-isothermal molecular dynamics simulations utilizing density functional theory: An assessment of the structure and density of water at near-ambient conditions," *Journal of Physical Chemistry B*, vol. 113, no. 35, pp. 11959–11964, 2009.